Growth and Structural Characterization of $Rb_2Ti_{1.01}Er_{0.99}(PO_4)_3$

J. J. Carvajal,† A. Aznar,† R. Solé,† Jna. Gavaldà,† J. Massons,† X. Solans,‡ M. Aguiló,† and F. Díaz*,†

Física i Cristal·lografia de Materials i IEA, Universitat Rovira i Virgili, Imperial Tàrraco, 1, 43005 Tarragona, Spain, and Departament de Cristal·lografia i Mineralogia, Universitat de Barcelona, 08028 Barcelona, Spain

Received August 1, 2002. Revised Manuscript Received October 16, 2002

We successfully grew langbeinite-type structures containing Ti^{4+} and Ln^{3+} ions as $M_2Ti_{2-x}Ln_x(PO_4)_3$ crystals (M = K^+ or Rb^+ and Ln = Er^{3+} or Yb^{3+}) by high-temperature-solution methods. We took accurate composition measurements of these crystals, paying special attention to the lanthanide contents. We resolved the structure of the $Rb_2Ti_{1.01}Er_{0.99}(PO_4)_3$ crystal and studied the evolution of this structure with the temperature. We found that this compound decomposed at 1323 K. We made a preliminary study to check the nonlinear optical properties of these materials, showing that the second-harmonic generation efficiency of the $Rb_2Ti_{1.01}Er_{0.99}(PO_4)_3$ was at least similar to that of potassium dihydrogen phosphate.

Introduction

Compounds that contain mixed-valence cations, for example, Ti^{3+}−Ti^{4+}, have interesting properties for catalysts, nonlinear optics, molecular sieves, ion exchangers, and ionic conductors.[1] In particular, langbeinite-type compounds, such as $M_xTi_2(PO_4)_3$ (M = Na^+, $x = 1-3$; M = K^+, $x = 1.5-2$; M = Rb^+,Tl^+, $x = 2$) have been used as superionic conductors.[2,3]

In the study of the crystallization region of $RbTiOPO_4$ (RTP) doped with Er or Yb and co-doped with Nb and Er or Nb and Yb (a material with important nonlinear optical properties and possibilities of a efficient laser emission),[4] new langbeinite structures with the general formula $Rb_2Ti_{2-x-y}Ln_xNb_y(PO_4)_3$ with Ln = Er or Yb have been found as boundary phases to these crystallization regions.

Langbeinite-type structures belong to cubic system with the $P2_13$ space group. The framework contains isolated PO_4 tetrahedra, each sharing its four corners with a TiO_6 octahedron. Reciprocally, the TiO_6 are isolated and linked to six PO_4 tetrahedra.[5] Incorporating lanthanide ions into this structure opens up a new application for these crystals: laser emission. Other langbeinite-type compounds containing lanthanide ions have already been grown, but this possibility was not pointed out.[6]

In this paper we study the possibilities of obtaining these types of structures from high-temperature solutions in the $Rb_2O-P_2O_5-TiO_2$ system, by partial substitution of TiO_2 with Ln_2O_3 or Nb_2O_5. We also did a parallel study to determine whether the same langbeinite phase can be obtained by completely substituting Rb with K. We carried out single-crystal diffraction analysis of $Rb_2Ti_{1.01}Er_{0.99}(PO_4)_3$ and determined its morphology. As this structure is not centrosymmetric, we made a preliminary study of the possibilities of second-harmonic generation.

Experimental Section

Crystal Growth and Identification of Crystalline Phases. It is difficult to obtain materials that contain transition metals with mixed valence. Methods in the literature include the reduction of the metal with the higher valence by adding metallic powder and maintaining the mixture at a high temperature for several days,[2] or controlling the oxidation of the initial metals, that are introduced with the lower valence.[1] However, only very small single crystals have been obtained so far. In our case, we did not use mixed-valence transition metals. Instead, we used two different metals with two different valences (Ti^{4+} and Er^{3+} or Yb^{3+}). This made it easier to grow these materials.

The crystal growth experiments were carried out in a vertical tubular furnace with a Kanthal AF heater. The temperature was controlled with a Eurotherm 818P controller/programmer connected to a thyristor. The temperature near the heater was measured with an S-type thermocouple.

We obtained langbeinite-type compounds when we studied the crystallization region of RTP in the $Rb_2O-P_2O_5-TiO_2$ system, with a partial substitution of TiO_2 by Er_2O_3 or Yb_2O_3 or combinations of Nb_2O_5 with one of these lanthanide oxides (see Table 1). In the literature, the RTP structure is traditionally studied parallel to its well-known isomorph KTP (the most used nonlinear optical material in doubling the near-IR laser emissions). We therefore carried out a systematic study for

* Corresponding author. E-mail: diaz@quimica.urv.es.
† Universitat Rovira i Virgili.
‡ Universitat de Barcelona.

(1) Zatovsky, I. V.; Slobodyanik, N. S.; Stratiychuk, D. A.; Domasevitch, K. V.; Sieler, J.; Rusanov, E. B. *Z. Naturforsch., B: Chem. Sci.* **2000**, *55*, 291.
(2) Leclaire, A.; Benmoussa, A.; Borel, M. M.; Grandin, A.; Raveau, B. *J. Solid State Chem.* **1989**, *78*, 227.
(3) Goodenough, J. B.; Hong, H. Y.-P.; Kafalas, J. A. *Mater. Res. Bull.* **1976**, *11*, 204.
(4) Carvajal, J. J.; Nikolov, V.; Solé, R.; Gavaldà, Jna.; Massons, J.; Aguiló, M.; Díaz, F. *Chem. Mater.* **2002**, *14*, 3136.
(5) Masse, R.; Durif, A.; Guitel, J. C.; Tordjman, I. *Bull. Soc. Fr. Minéral. Cristallogr.* **1972**, *95*, 47.
(6) Wulff, H.; Guth, U.; Loescher, B. *Powder Diffr.* **1992**, *7*, 103.

10.1021/cm020806t CCC: $25.00 © 2003 American Chemical Society
Published on Web 12/05/2002

Table 1. Solution Compositions Studied and the Chemical Composition of the Crystals Obtained

exp. number	solution composition (mol %) Rb_2O	K_2O	P_2O_5	TiO_2	Er_2O_3	Yb_2O_3	Nb_2O_5	crystal composition	crystal color
1	44.8	0	33.1	22.0	0	0	0	$RbTiOPO_4$	colorless
2	44.8	0	33.1	21.1	0	0.9	0	$Rb_{2.06}Ti_{0.98}Yb_{1.02}(PO_4)_3$	colorless
3	43.1	0	31.9	25.0	0	0	0	$RbTiOPO_4$	colorless
4	43.1	0	31.9	24.0	1.0	0	0	$RbTi_{0.997}Er_{0.003}OPO_4$	pale pink
5	43.1	0	31.9	23.5	1.5	0	0	$RbTi_{0.996}Er_{0.005}OPO_4$	pale pink
								$Rb_{1.99}Ti_{0.84}Er_{1.16}(PO_4)_3$	pink
6	43.1	0	31.9	23.0	2.0	0	0	$Rb_{1.99}Ti_{0.80}Er_{1.20}(PO_4)_3$	pink
7	43.1	0	31.9	23.2	1.2	0	0.5	$Rb_{2.00}Ti_{0.76}Er_{1.17}Nb_{0.07}(PO_4)_3$	pink
8	43.1	0	31.9	23.0	1.0	0	1.0	$Rb_{2.01}Ti_{0.64}Er_{1.19}Nb_{0.17}(PO_4)_3$	pink
9	43.1	0	31.9	22.5	1.0	0	1.5	$Rb_{2.01}Ti_{0.53}Er_{1.23}Nb_{0.24}(PO_4)_3$	pink
10	43.1	0	31.9	22.0	1.0	0	2.0	$Rb_{2.02}Ti_{0.45}Er_{1.28}Nb_{0.27}(PO_4)_3$	pink
11	43.1	0	31.9	21.7	1.0	0	2.2	$Rb_{2.03}Ti_{0.43}Er_{1.27}Nb_{0.30}(PO_4)_3$	pink
12	43.1	0	31.9	23.5	0	1.5	0	$Rb_{2.05}Ti_{0.81}Yb_{1.19}(PO_4)_3$	colorless
13	43.1	0	31.9	23.2	0	0.7	1.0	$Rb_{2.07}Ti_{0.65}Yb_{1.18}Nb_{0.17}(PO_4)_3$	colorless
14	43.1	0	31.9	22.7	0	0.7	1.5	$Rb_{2.08}Ti_{0.61}Yb_{1.22}Nb_{0.17}(PO_4)_3$	colorless
15	43.1	0	31.9	22.2	0	0.7	2.0	$Rb_{2.12}Ti_{0.47}Yb_{1.27}Nb_{0.26}(PO_4)_3$	colorless
16	43.1	0	31.9	22.2	0	0.5	2.2	$Rb_{2.12}Ti_{0.46}Yb_{1.25}Nb_{0.29}(PO_4)_3$	colorless
17	42.9	0	35.1	22.0	0	0	0	$RbTiOPO_4$	colorless
18	42.9	0	35.1	21.6	0.4	0	0	$RbTiOPO_4$	pale pink
19	42.9	0	35.1	21.3	0.7	0	0	$Rb_{1.93}Ti_{1.01}Er_{0.99}(PO_4)_3$	violet
20	42.9	0	35.1	20.9	1.1	0	0	$Rb_2Ti_{1.01}Er_{0.99}(PO_4)_3$	violet
21	42.9	0	35.1	21.1	0	0.9	0	$Rb_2Ti_{0.98}Yb_{1.02}(PO_4)_3$	colorless
22	40.8	0	27.2	29.1	0	1.6	1.3	$RbTiOPO_4$	colorless
								$Rb_{1.97}Ti_{0.48}Yb_{1.38}Nb_{0.14}(PO_4)_3$	colorless
23	40.8	0	27.2	28.8	0	1.9	1.3	$Rb_{1.97}Ti_{0.45}Yb_{1.43}Nb_{0.12}(PO_4)_3$	colorless
24	40.8	0	27.2	29.1	0	1.3	1.6	$RbTiOPO_4$	colorless
								$Rb_{1.97}Ti_{0.48}Yb_{1.39}Nb_{0.13}(PO_4)_3$	colorless
25	40.2	0	29.7	30.0	0	0	0	$RbTiOPO_4$	colorless
26	40.2	0	29.7	28.5	0	1.5	0	$Rb_{2.08}Ti_{0.81}Yb_{1.18}(PO_4)_3$	colorless
27	37.0	0	37.0	26.0	0	0	0	$Rb_3Ti_3O(P_2O_7)(PO_4)_3$	colorless
28	37.0	0	37.0	25.2	0.8	0	0	$Rb_{1.89}Ti_{1.10}Er_{0.90}(PO_4)_3$	violet
29	37.0	0	37.0	24.6	1.4	0	0	$Rb_{1.92}Ti_{1.06}Er_{0.94}(PO_4)_3$	violet
30	37.0	0	37.0	23.7	2.3	0	0	$ErPO_4$	pink
31	0	37.4	41.5	21.0	0	0	0	$KTi_2(PO_4)_3$	colorless
32	0	37.4	41.5	20.3	0.6	0	0	$K_{0.96}Ti_{1.97}Er_{0.02}(PO_4)_3$	pale pink
33	0	37.4	41.5	19.9	1.1	0	0	$K_{0.97}Ti_{1.97}Er_{0.02}(PO_4)_3$	pale pink
34	0	37.4	41.5	19.2	1.8	0	0	$K_{1.78}Ti_{1.15}Er_{0.85}(PO_4)_3$	violet

obtaining the Er-containing langbeinite structure by completely substituting Rb with K (also see Table 1). Rb_2CO_3, K_2CO_3, $NH_4H_2PO_4$, TiO_2, and Nb_2O_5 with purities of above 99% and Er_2O_3 or Yb_2O_3 with purities of above 99.9% were used as starting reagents.

The solutions, which weighed about 20 g, were prepared in platinum crucibles of 25 cm^3. We mixed and decomposed the initial reagents by heating them until the bubbling of NH_3, H_2O, and CO_2 was complete. The solutions were homogenized for several hours at temperatures of 1313−1353 K. The axial thermal gradient was about 15−20 K/cm, hot bottom.

When the solution was homogeneous, we decreased the temperature in 10 K steps every 30 min until crystals appeared on a platinum wire immersed in the solution. We then decreased the temperature between 10 and 20 K at a rate of 1−2.5 K/h to obtain a higher amount of macroscopic crystals. The phase that crystallized from each solution composition was preliminarily identified by direct observation in an optical microscope and then by X-ray powder diffraction analyses using a Siemens D-5000 X-ray powder diffractometer. We observed some of these crystals in greater detail and photographed them in a scanning electron microscope (SEM) JEOL JSM 6400.

EPMA Measurements. We analyzed the chemical composition of the crystals by electron probe microanalyses with wavelength-dispersion spectroscopy (EPMA-WDS) in a CAMECA SX-50 operating at 25-kV accelerating voltage and 30-nA electron current for Rb, Ti, P, and O and 100 nA for Er, Yb, and Nb. We used an RTP crystal, grown by us, as the standard for measuring Rb, Ti, P, and O and a synthetic glass (REE1) containing 4.09 mol % of Er as standard for Er, YbF_3 for Yb, and $LiNbO_3$ for Nb. The analyses were made using the lines Rb Lα and P Kα measured with the TAP crystal, Ti Kα and Nb Lα measured with the PET crystal, O Kα measured with a W/Si multilayer crystal ($2d = 60$ Å), and Er Lα and Yb Lα measured with the LiF crystal. The measurements were integrated for 10 s for Rb, Ti, P, and O and 30 s for Er, Yb, and Nb. The accuracy of the measurements was 1.2% for K, Rb, and Ti, 1.4% for P, 2.6% for O, 3.37% for Nb, 2.4% for Er, and 1.1% for Yb. We corrected the raw intensities for the effects of dead time, background, and matrix using the PAP correction procedure.[7]

X-ray Diffraction. We performed single-crystal X-ray diffraction using a MAR-Research MAR-345 diffractometer on an as-grown single crystal of $Rb_2Ti_{1.01}Er_{0.99}OPO_4$ and resolved the structure by Patterson synthesis. Tables 2−4 show details on crystal data, data collection, and refinement.

We performed X-ray powder diffraction studies of $Rb_2Ti_{0.81}Yb_{1.19}(PO_4)_3$ using Cu Kα radiation collected on a Siemens D5000 powder diffractometer in a $\theta-\theta$ goniometer using Bragg−Brentano parafocusing geometry. The goniometer was fitted with a curved graphite diffracted-beam monochromator and a scintillation counter as the detector. The cell parameters of the crystals and the occupation factors were calculated from the powder diffraction data obtained at $2\theta = 10-70°$, ss = 0.03°, st = 5 s, at 298 K. The structure of $Rb_2Ti_{1.01}Er_{0.99}(PO_4)_3$, obtained by single-crystal X-ray diffraction, was used as the starting model for refining the structure of $Rb_2Ti_{0.81}Yb_{1.19}(PO_4)_3$.

To study the linear thermal expansion tensor of $Rb_2Ti_{1.01}Er_{0.99}(PO_4)_3$, we performed X-ray powder diffraction studies with the previously mentioned equipment equipped with an Anton-Paar HTK10 platinum ribbon heating stage. The cell parameters of the crystals were calculated from the powder

(7) Pouchou, J. L.; Pichoir, F. *Rech. Aerosp.* **1984**, *3*, 13.

Table 2. Crystal Data, Data Collection, and Refinement of $Rb_2Ti_{1.01}Er_{0.99}(PO_4)_3$

Crystal Data	
$Rb_2Ti_{1.01}Er_{0.99}(PO_4)_3$	Mo Kα radiation
formula weight = 669.22	λ = 0.71069 Å
cubic	cell parameters from 10798 reflections
$P2_13$	θ = 2.84−33.12°
a = 10.1580(10) Å	μ = 18.355 mm^{-1}
$\alpha = \beta = \gamma$ = 90°	T = 293(2) K
	equidimensional
	0.2-mm diameter
V = 1048.15(18) $Å^3$	violet
Z = 4	
D_x = 4.241 Mg m^{-3}	
D_m = (not measured)	
Data Collection	
MAR-Research MAR-345 diffractometer	R_{int} = 0.025
φ-scan	θ_{max} = 33.12°
absorption correction: φ-scan	h = 1→15
10798 measured reflections	k = 0→11
741 independent reflections	l = 0→10
740 reflections with $I > 2\sigma(I)$	
Refinement	
refinement on F^2 $R[F^2 > 2\sigma(F^2)]$ = 0.0354	$\Delta\rho_{max}$ = 0.666 e $Å^{-3}$
w$R(F^2)$ = 0.0878	$\Delta\rho_{min}$ = −0.665 e $Å^{-3}$
S = 1.118	extinction correction method: SHELXL
741 reflections	extinction coefficient = 0.0088(9)
61 parameters	Flack absolute structure parameter = 0.09(3)
$w = 1/[\sigma^2(F_o^2) + (0.0356P)^2 + 19.9026P]$ where $P = (F_o^2 + 2F_c^2)/3$	scattering factors from *Internacional Tables for Crystallography* (Vol. C)
$(\Delta/\sigma)_{max}$ = 0.001	

Table 3. Atomic Coordinates and Equivalent Isotropic Displacement Parameters of $Rb_2Ti_{1.01}Er_{0.99}(PO_4)_3$

atom	Wyckoff position	x	y	z	occupation factor	U(eq)
Ti(1)	4a	0.6666(1)	0.6666(1)	0.6666(1)	0.358(7)	0.006(1)
Er(1)	4a	0.6666(1)	0.6666(1)	0.6666(1)	0.642(7)	0.006(1)
Ti(2)	4a	0.3981(1)	0.3981(1)	0.3981(1)	0.655(7)	0.007(1)
Er(2)	4a	0.3981(1)	0.3981(1)	0.3981(1)	0.345(7)	0.007(1)
P	12b	0.4847(2)	0.7081(2)	0.3717(2)	1	0.012(1)
Rb(1)	4a	0.9584(1)	0.9584(1)	0.9584(1)	1	0.019(1)
Rb(2)	4a	0.1797(1)	0.1797(1)	0.1797(1)	1	0.016(1)
O(1)	12b	0.6000(9)	0.8447(9)	0.7445(8)	1	0.028(2)
O(2)	12b	0.4554(10)	0.2874(11)	0.2388(10)	1	0.037(2)
O(3)	12b	0.4840(9)	0.5621(9)	0.3318(9)	1	0.029(2)
O(4)	12b	0.5693(12)	0.7307(9)	0.4946(10)	1	0.036(2)

Table 4. Anisotropic Displacement Parameters ($Å^2$) of Cubic $Rb_2Ti_{1.01}Er_{0.99}(PO_4)_3$[a]

atom	U_{11}	U_{22}	U_{33}	U_{23}	U_{13}	U_{12}
Ti(1)	0.006(1)	0.006(1)	0.006(1)	−0.001(1)	−0.001(1)	−0.001(1)
Er(1)	0.006(1)	0.006(1)	0.006(1)	−0.001(1)	−0.001(1)	−0.001(1)
Ti(2)	0.007(1)	0.007(1)	0.007(1)	0	0	0
Er(2)	0.007(1)	0.007(1)	0.007(1)	0	0	0
Rb(1)	0.019(1)	0.019(1)	0.019(1)	−0.001(1)	−0.001(1)	−0.001(1)
Rb(2)	0.016(1)	0.016(1)	0.016(1)	−0.002(1)	−0.002(1)	−0.002(1)
P	0.016(1)	0.012(1)	0.009(1)	0	−0.001(1)	−0.002(1)
O(1)	0.028(4)	0.028(4)	0.026(4)	−0.009(3)	0.001(3)	−0.009(3)
O(2)	0.029(4)	0.050(6)	0.032(5)	−0.021(5)	0.004(4)	−0.003(4)
O(3)	0.033(4)	0.028(4)	0.027(4)	−0.015(3)	0	0.013(3)
O(4)	0.053(6)	0.027(4)	0.028(4)	0	−0.020(4)	−0.011(4)

[a] The anisotropic displacement factor exponent takes the following form: $-2\pi^2[h^2a^{*2}U_{11} + ... + 2hka^*b^*U_{12}]$.

diffraction data obtained at 2θ = 10−70°, ss = 0.03°, st = 5 s, at 298, 323, 373, 473, 573, 673, and 773 K. We increased the temperature at a rate of 5 K/s and introduced a delay of 1800 s before starting each pattern at each temperature.

In all of these experiments, the crystal cell parameters and occupation factors for $Rb_2Ti_{0.81}Yb_{1.19}(PO_4)_3$ were refined with the FULLPROF program[8] and the Rietveld method.[9] We used the coordinates of the atoms from the structure resolved with single-crystal X-ray diffraction (see Table 3) as the starting model for the calculations and selected a Pearson VII function to describe individual line profiles.

We took another series of measurements to study the evolution of the material with the temperature using X-ray powder diffraction. The patterns were carried out using Cu Kα radiation collected on a Siemens D5000 powder diffractometer in a $\theta-\theta$ goniometer using Bragg−Brentano parafocusing geometry equipped with an Anton-Paar HTK10 platinum ribbon heating stage and a Braun position-sensitive detector (PSD). The powder diffraction data were obtained at 2θ = 10−70°, and the measuring time per degree was 10 s in the 298−1473 K range. We increased the temperature at a rate of 0.17 K/s and registered patterns every 50 K.

(8) Rodriguez-Carvajal, J. *Physica B* **1993**, *192*, 55.
(9) Young, R. A. *The Rietveld Method*; Oxford Science Publication, International Union of Crystallography: Oxford, U.K., 1995.

Table 5. Selected Interatomic Distances (in Å) in $Rb_2Ti_{1.01}Er_{0.99}(PO_4)_3$

P−O(2)^{i}	1.509(10)	Ti(1)−O(1)	2.087(9)	Er(1)−O(1)	2.087(9)	Rb(1)−O(3)^{iii}	2.966(9)	Ti(1)−P^{iii}	3.495(2)
P−O(1)^{ii}	1.529(9)	Ti(1)−O(4)	2.111(10)	Er(1)−O(4)	2.111(10)	Rb(1)−O(4)^{iv}	3.192(10)	Ti(1)−P	3.545(2)
P−O(4)	1.532(10)					Rb(1)−O(2)^{iii}	3.269(12)		
P−O(3)	1.538(9)	Ti(2)−O(3)	1.998(11)	Er(2)−O(3)	1.998(11)	Rb(1)−O(2)^{v}	3.460(12)	Ti(2)−P	3.281(2)
		Ti(2)−O(2)	2.055(9)	Er(2)−O(2)	2.055(9)			Ti(2)−P^{vii}	3.557(2)
						Rb(2)−O(1)^{vi}	2.927(9)		
						Rb(2)−O(2)	3.065(10)	Rb(1)−P^{iv}	3.548(2)
						Rb(2)−O(4)^{vii}	3.147(12)	Rb(1)−P^{iii}	3.765(2)
						Rb(2)−O(4)^{vi}	3.280(12)	Rb(1)−Ti(2)^{viii}	3.9510(13)
								Rb(1)−Ti(1)^{ix}	4.5386(12)
								Rb(2)−P^{vii}	3.461(2)
								Rb(2)−P^{vi}	3.725(2)
								Rb(2)−Ti(2)	3.8413(11)
								Rb(2)−Ti(1)^{x}	3.8509(10)

i = $1 - x$, $^1/_2 + y$, $^1/_2 - z$. ii = $y - ^1/_2$, $^3/_2 - z$, $1 - x$. iii = $^3/_2 - y$, $1 - z$, $x + ^1/_2$. iv = $2 - y$, $z + ^1/_2$, $^3/_2 - x$. v = $1 - y$, $z + ^1/_2$, $^3/_2 - x$. vi = $1 - y$, $z - ^1/_2$, $^1/_2 - x$. vii = $y - ^1/_2$, $^1/_2 - z$, $1 - x$. viii = $1 - z$, $x + ^1/_2$, $^3/_2 - y$. ix = $^3/_2 - x$, $2 - y$, $z + ^1/_2$. x = $^1/_2 - x$, $1 - y$, $z - ^1/_2$.

Differential Thermal Analysis (DTA) Measurements. We also studied the phase transitions with the temperature by differential thermal analysis, using a TA Instruments Simultaneous Differential Techniques Instrument SDT 2960. The experiments were made at 10 K/min in the 298−1473 K range using Ar as the purge gas at a flow rate of 90 cm^3/min. The sample of $Rb_2Ti_{1.01}Er_{0.99}(PO_4)_3$, which weighed around 30 mg, was placed in Pt pans. We used calcined Al_2O_3 as the reference material. The experiments were made by heating and cooling cycles to obtain information about the reversibility of the phase transitions. The storage rate of data was always 0.5 s/data point.

Second-Harmonic Generation (SHG) Measurements. We studied the second-harmonic generation (SHG) response of $Rb_2Ti_{1.01}Er_{0.99}(PO_4)_3$ using the Kurtz method.[10] The samples were powdered and graded using standard sieves to obtain a uniform particle size between 5 and 20 μm. The sample was then placed in a 2-mm-thick quartz cell and packed uniformly. The incident radiation on the sample was generated by a pulsed YAG:Nd laser and we estimated the incident power by measuring the energy reflected by the sample with a Si detector. We also measured the energy of the radiation from the sample, the frequency of which was double the initial frequency, with a Si detector. We selected the desired signal using interferometer filters. The initial and the double frequency signals were compared, and the ratio between these two signals provided information about the efficiency of the second-harmonic generation process. The ratio between these two signals was calculated as an average over 100 laser shots.

We only obtain relative values of SHG efficiency of the sample with this method. These values will be compared with those of $KTiOPO_4$ (KTP) and KH_2PO_4 (KDP), which are both well-known in the literature.[11]

Results and Discussion

Crystal Growth. We grew crystals of langbeinite structure with typical dimensions between a few micrometers and a few millimeters. Table 1 shows the phases crystallized, the level of Ln and Nb introduction in the samples, and the color of the crystals. As the table shows, the crystals were obtained from various solution compositions, indicating as initial solution composition when TiO_2 has not been yet substituted by Ln_2O_3 or Nb_2O_3. In all these solutions we progressively substituted part of TiO_2 with Er_2O_3, Yb_2O_3, or combinations of Er_2O_3 and Nb_2O_5 or Yb_2O_3 and Nb_2O_5. Some of these solution compositions were located in the crystallization region of RTP,[12] corresponding to an initial solution composition of $Rb_2O-P_2O_5-TiO_2$ = 44.8−33.1−22.0 (experiments 1 and 2), 43.1−31.9−25.0 (experiments 3−16), 42.9−35.1−22.0 (experiments 17−21), 40.8−27.2−32.0 (experiments 22−24), and 40.2−29.7−30.0 (experiments 25 and 26). We chose another initial solution composition in the crystallization region of $Rb_3Ti_3O(P_2O_7)(PO_4)_3$ (experiments 27−30), a neighboring phase of the RTP in the system $Rb_2O-P_2O_5-TiO_2$,[12] which corresponds to an initial solution composition of 37.0−37.0−26.0. Finally, because of the historical parallelism studies between RTP and KTP, we chose a solution in which Rb_2O was completely substituted by K_2O to investigate whether we could obtain the langbeinite structure with K instead of with Rb. This solution corresponded to an initial composition of $K_2O-P_2O_5-TiO_2$ = 37.4−41.5−21.0 (experiments 31−34) and is located in the crystallization region of $KTi_2(PO_4)_3$.[13]

For initial solutions chosen inside the crystallization region of RTP, the langbeinite phase stabilized when the P_2O_5 content was increased and the global content of TiO_2 and substituents in the solution was decreased. When Nb_2O_5 was present in the solution, the langbeinite phase was stabilized by a lower substitution of TiO_2 by Ln_2O_3.

For the initial solution composition located in the crystallization region of $Rb_3Ti_3O(P_2O_7)(PO_4)_3$, the langbeinite phase was stable at least from a concentration of Er_2O_3 of 3 mol % substituting TiO_2 to almost 8 mol %, where $ErPO_4$ was identified, while in the system containing K_2O, the langbeinite phase was stable from a concentration of Er_2O_3 of 5 to almost 8 mol %. Then, the langbeinite structure was stabilized for low quantities of Er_2O_3 in the system with Rb_2O.

EPMA Measurements. The chemical composition of these crystals was analyzed by EPMA. It seems that these structures incorporate the Ln^{3+} more easily than the Nb^{5+}, even though the ionic radius of the latter is closer to that of Ti^{4+} than that of Ln^{3+}. In these crystals, it becomes increasingly important to substitute Ti^{3+} in the framework with an ion of the same electronic valence than with an ion with an ionic radii closer to that of Ti^{3+}. As an example, when the solution only contained Ln_2O_3, the higher the concentration of Ln_2O_3

(10) Kurtz, S. K.; Perry, T. T. *J. Appl. Phys.* **1968**, *39*, 3798.
(11) Dmitriev, V. G.; Gurzadyan, G. G.; Nikogosyan, D. N. *Handbook of Nonlinear Optical Materials*; Springer-Verlag: New York, 1991.
(12) Carvajal, J. J.; Nikolov, V.; Solé, R.; Gavaldà, Jna.; Massons, J.; Rico, M.; Zaldo, C.; Aguiló, M.; Díaz, F. *Chem. Mater.* **2000**, *12*, 3171.
(13) Iliev, K.; Peshev, P.; Nikolov, V.; Koseva, I. *J. Cryst. Growth* **1990**, *100*, 225.

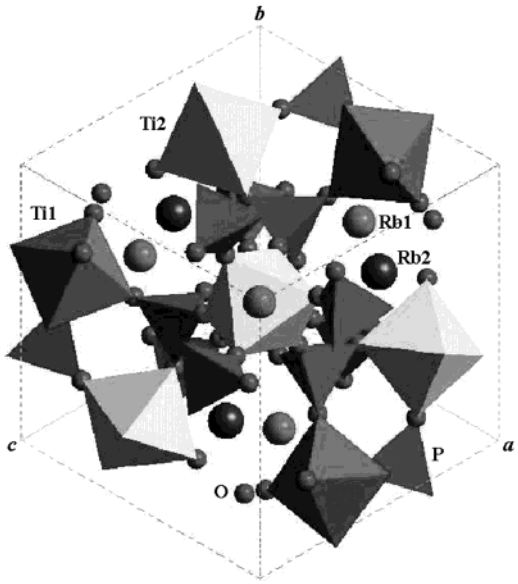

Figure 1. View of the TiO_6 octahedra and PO_4 tetrahedra in the structure of $Rb_2Ti_{1.01}Er_{0.99}(PO_4)_3$.

in the solution, the higher the concentration of Ln^{3+} in the crystals (see experiments 5−6 and 28−29). When Nb_2O_5 was present in the solution, the higher the concentration of Nb_2O_5 in the solution, the higher the atomic content of Nb^{5+} in the crystals and higher the incorporation of Ln^{3+} into the crystals (see experiments 7−11 or experiments 13−15). Finally, for solutions containing the same concentrations of Nb_2O_5, the higher the concentration of Ln_2O_3 in the initial solution, the higher the content of Ln^{3+} in the crystal, but the lower the concentration of Nb in the crystals (see experiments 22 and 23).

In the samples containing Rb^+ and Er^{3+}, a change of color of the crystals with the Er content has been observed. Crystals with langbeinite structure whose content of Er^{3+} was less than 1% were violet (see experiments 19, 20, 28, and 29), and those whose content of Er^{3+} was more than 1% were pink (see experiments 6−12). Following the principle of electrical neutrality, this change in color may have been due to the presence of Ti^{3+} in the crystals whose content of Er^{3+} is less than 1%. The combination of the pink color for Er^{3+} and the blue for Ti^{3+} formed the violet color observed.

Crystal Structure of $Rb_2Ti_{1.01}Er_{0.99}(PO_4)_3$. The structure of $Rb_2Ti_{1.01}Er_{0.99}(PO_4)_3$ has been solved. The unit cell parameters obtained in this study were a = 10.1580(10) Å and Z = 4, with the space group of symmetry $P2_13$. This cell parameter was larger than the one corresponding to $Rb_2Ti_2(PO_4)_3$ (a = 9.9115 Å)[1] because the ionic radium of Er^{3+} is larger than the corresponding one of Ti^{3+} (0.670 Å for Ti^{3+} and 0.890 Å for Er^{3+}).[14] The atomic coordinates, mean interatomic lengths, and anisotropic thermal displacement parameters are shown in Tables 3−5.

Figure 1 shows a projection parallel to [111] of the cell contents of $Rb_2Ti_{1.01}Er_{0.99}(PO_4)_3$. There were two different structural positions of titanium and rubidium in the structure and four inequivalent O positions. The

(14) Shannon, R. D. *Acta Crystallogr., Sect. A: Found. Crystallogr.* **1976**, *32*, 751.

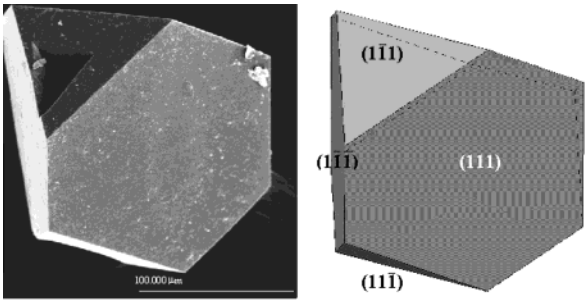

Figure 2. SEM photographs of a $Rb_2Ti_{1.01}Er_{0.99}(PO_4)_3$ crystal and morphological scheme made with *Shape* application.

Ti atoms were placed at 3-fold axes and were six-coordinated with oxygen atoms to form an octahedron. These polyhedra were different for each structural position. This is reflected in the different bond distances of Ti−O, where those corresponding to the $Ti(1)O_6$ octahedron were larger than those corresponding to the $Ti(2)O_6$ octahedron. In $Ti(1)O_6$ octahedra, the Ti−O distances ranged from 2.087 to 2.111 Å, whereas in the $Ti(2)O_6$ octahedra, they ranged from 1.998 to 2.055 Å. These results disagree with those of Leclaire et al.[2] for $K_2Ti_2(PO_4)_3$, where the larger cage was in the Ti(2) position, but no Er was present in these crystals. The $Ti(2)O_6$ octahedron seems to be more distorted than the $Ti(1)O_6$ octahedron because the distortion parameter $\Delta_d = (1/6)\sum_{n=1,6}[(d_n - \langle d\rangle)/\langle d\rangle]^2$, where d_n are the different distances of Ti−O in the octahedron and $\langle d\rangle$ is the mean Ti−O distance calculated in each octahedron, was higher than that of the $Ti(1)O_6$ octahedron (1.98×10^{-4} and 0.27×10^{-4}, respectively). This supposition is confirmed by the larger angle in the octahedra. Whereas in a regular octahedron this O−Ti−O angle is 180°, in the $Ti(1)O_6$ octahedron it is 174.4° and in $Ti(2)O_6$ it is 172.5°. Er generally preferred to occupy the Ti(1) site as can be seen in Table 3 where the occupation factors for Ti(1) and Ti(2) positions were Ti(1) = 0.358(7), Er-(1) = 0.642(7) and Ti(2) = 0.655(7), Er(2) = 0.345(7). This may be because of the larger Ti−O distances in the environment of the Ti(1) site with respect to the Ti-(2) site, which make a larger cage in the Ti(1) site than in the Ti(2) site. Our results also clearly show that pure sites for Ti^{3+} and Ti^{4+} do not exist and that both positions Ti(1) and Ti(2) were differently occupied by both ions with different valences. These octahedra were isolated in the structure and shared all six corners with PO_4 tetrahedra at two Ti−P distances ranging from 3.495 to 3.545 Å for $Ti(1)O_6$ and from 3.281 to 3.557 Å for $Ti(2)O_6$ (see Table 5).

The shortest distances in the structure were those that made up the coordination figure of the phosphate anion. This figure was a slightly distorted tetrahedron with distances ranging from 1.509 to 1.538 Å. These PO_4 tetrahedra were isolated in the structure and shared their four corners with TiO_6 octahedra. An isolated PO_4 tetrahedron shared two corners with $Ti(1)O_6$ octahedra and two corners with $Ti(2)O_6$ octahedra (see Figure 1).

Two different Rb^+ ions in the structure were linked to 12 oxygens at a distance ranging from 2.927 to 3.460 Å. The distance between the Rb(2) atom and the 12 oxygens that surround this ion in the structure were significantly shorter than the same distances for the Rb-(1) atom. Around these Rb ions there were six TiO_6

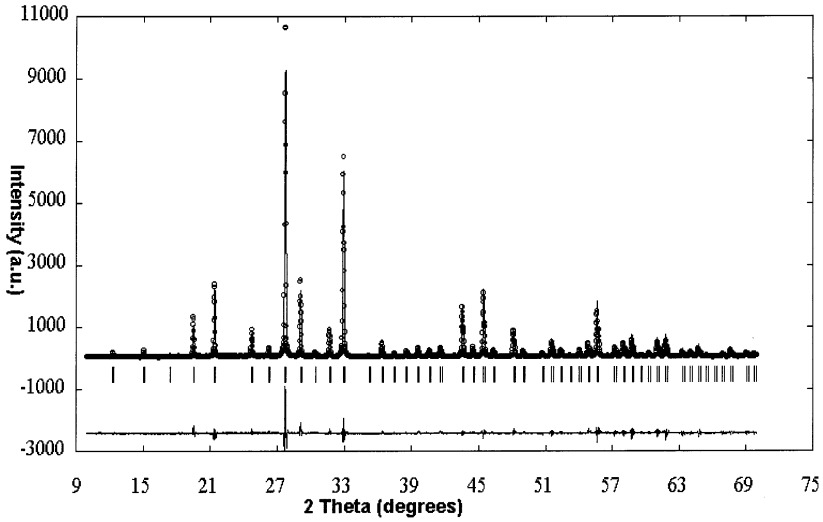

Figure 3. Refined X-ray powder diffraction pattern of $Rb_2Ti_{1.01}Er_{0.99}(PO_4)_3$ showing the observed (points), calculated (full line), and the difference (bottom) Rietveld profiles at RT.

Table 6. *hkl* Reflections, d_{hkl}, 2θ-Bragg Position, and Their Observed Intensity in the X-ray Powder Diffraction Pattern of $Rb_2Ti_{1.01}Er_{0.99}(PO_4)_3$ Crystal[a]

hkl	d_{hkl} (Å)	2θ-Bragg	I_{hkl}	*hkl*	d_{hkl} (Å)	2θ-Bragg	I_{hkl}
110	7.1944	12.292	10	521	1.8576	48.996	19
111	5.8742	15.070	10	440	1.7986	50.715	9
200	5.0872	17.418	1	441	1.7711	51.558	64
210	4.5502	19.493	105	530	1.7449	52.392	27
211	4.1537	21.374	197	135	1.7198	53.217	2
220	3.5972	24.729	86	600	1.6957	54.032	27
221	3.3915	26.255	38	610	1.6727	54.840	56
310	3.2175	27.703	999	611	1.6505	55.639	212
311	3.0677	29.084	242	620	1.6087	57.216	37
222	2.9371	30.408	21	621	1.5890	57.994	60
320	2.8219	31.682	85	541	1.5700	58.765	83
123	2.7192	32.911	639	533	1.5516	59.530	7
400	2.5436	35.255	<1	622	1.5339	60.289	19
014	2.4677	36.377	40	542	1.5167	61.043	77
411	2.3981	37.471	6	136	1.5001	61.791	81
331	2.3342	38.537	20	444	1.4686	63.271	25
024	2.2751	39.580	29	236	1.4535	64.004	21
124	2.2203	40.600	22	543	1.4389	64.733	44
332	2.1692	41.599	35	551	1.4247	65.457	4
422	2.0769	43.541	183	046	1.4109	66.177	2
034	2.0349	44.486	36	720	1.3976	66.893	13
431	1.9954	45.416	243	127	1.3846	67.605	35
511	1.9581	46.331	24	246	1.3596	69.019	20
234	1.8894	48.120	104	722	1.3476	69.720	15

[a] The observed intensity has been normalized taking 999 as the most intense reflection.

octahedra, three of which were at a shorter distance than the others, and all distances were shorter for Rb-(2) than for Rb(1). These TiO_6 octahedra were located at two different distances with respect to each Rb center. The Rb atoms were also surrounded by six PO_4 tetrahedra at a distance ranging from 3.461 to 3.765 Å. Again, the distances between Rb and P centers were shorter for Rb(2) than for Rb(1) (see Table 5).

Crystal Structure of $Rb_{2.05}Ti_{0.81}Yb_{1.19}(PO_4)_3$. Using the above-described structural model as a starting point and substituting Er with Yb, we tried to solve the structure of $Rb_{2.05}Ti_{0.81}Yb_{1.19}(PO_4)_3$ from X-ray powder diffraction data using the FULLPROF program. We found that the cell parameter was $a = 10.2294(1)$ Å, which is slightly different from the one for $Rb_2Ti_{1.01}Er_{0.99}(PO_4)_3$. This may be because the concentration of Yb in $Rb_{2.05}Ti_{0.81}Yb_{1.19}(PO_4)_3$ was higher than the concentration of Er in $Rb_2Ti_{1.01}Er_{0.99}(PO_4)_3$, even though the

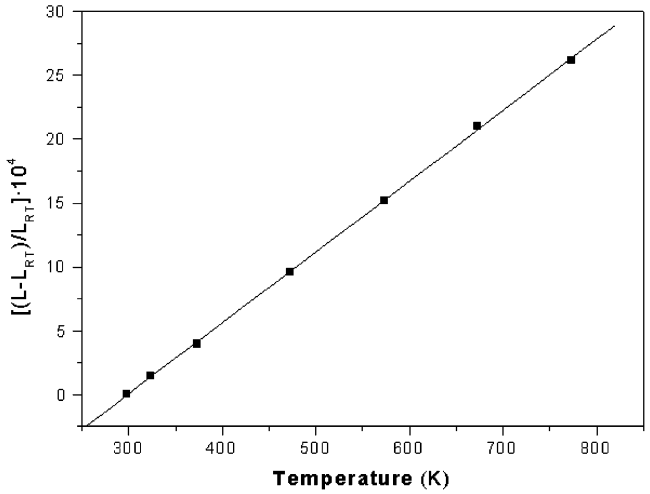

Figure 4. Linear thermal expansion of the cell parameter of the $Rb_2Ti_{1.01}Er_{0.99}(PO_4)_3$ crystal in the range between 300 and 800 K.

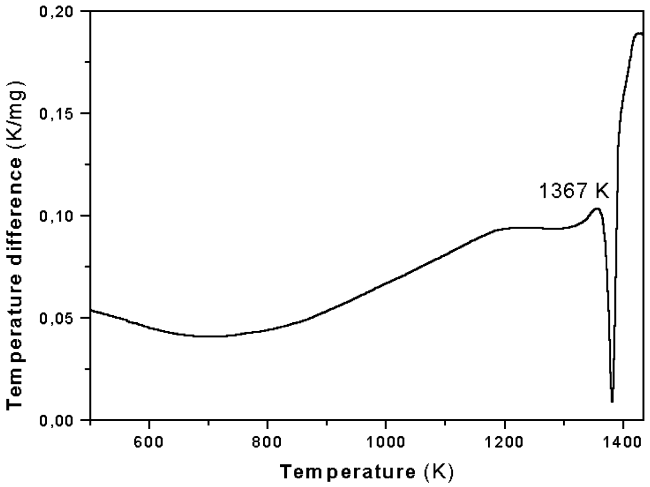

Figure 5. Differential thermal analysis (DTA) thermogram of $Rb_2Ti_{1.01}Er_{0.99}(PO_4)_3$ in the range between 500 and 1450 K.

ionic radius of Yb^{3+} in an octahedral environment is smaller than the ionic radius of Er^{3+} (0.868 and 0.890 Å, respectively).[14] We found that the occupation factor of Yb in the structure showed the same tendency as in

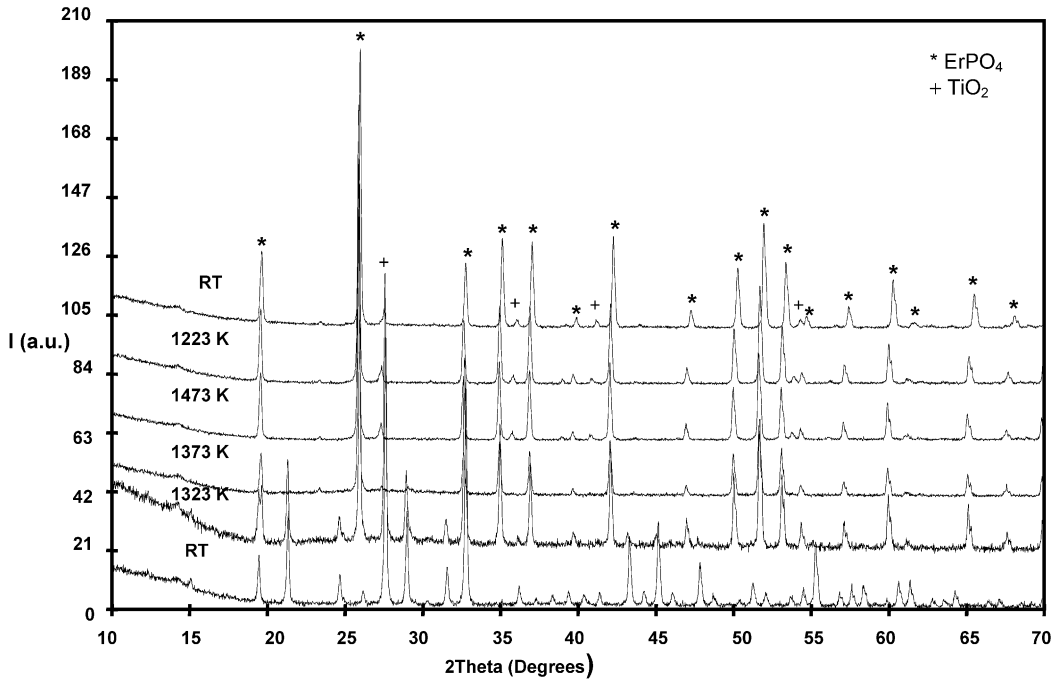

Figure 6. Selected X-ray powder patterns at different temperatures describing the decomposition of $Rb_2Ti_{1.01}Er_{0.99}(PO_4)_3$ around 1373 K.

$Rb_2Ti_{1.01}Er_{0.99}(PO_4)_3$: the Yb^{3+} were located more at the Ti(1) position than at the Ti(2) position. The occupation factors in this structure in Ti(1) and Ti(2) positions were Ti(1) = 0.258(2), Yb(1) = 0.741(2) and Ti(2) = 0.555(2), Yb(2) = 0.444(2).

Crystal Morphology. We observed our crystals by scanning electron microscopy (SEM) to describe their morphology. The habit of the crystals was made up of hexagons and triangles, basically comprising the {111} and $\{11\bar{1}\}$ faces. These were not equivalent by symmetry because as the theoretical simulation made with the Shape software shows,[15] there was no mirror plane in this structure. The habit of these crystals, grown by spontaneous nucleation on the surface of the solution, is shown in Figure 2. In this figure we can also see the different development of the {111} and $\{11\bar{1}\}$ forms.

Thermal Expansion Coefficient. We studied the evolution of the *a* parameter of the $Rb_2Ti_{1.01}Er_{0.99}(PO_4)_3$ by X-ray powder diffraction in the 300−800 K temperature range using the FULLPROF program. Figure 3 shows the X-ray diffraction pattern of $Rb_2Ti_{1.01}Er_{0.99}(PO_4)_3$ refined by FULLPROF at room temperature. As there was no powder diffraction file corresponding to this structure in the JCPDF-ICDD database, Table 6 lists (*hkl*), d_{hkl}, 2θ-Bragg position, and the corresponding I_{hkl} observed. Figure 4 shows the results of the thermal expansion of this structure. The linear thermal expansion coefficient is defined as $\alpha = (1/L) \times (\Delta L/\Delta T)$, where L is the initial parameter at room temperature and ΔL is the change in this parameter when the temperature changes ΔT. From our measurements of the lattice parameters, we can calculate the thermal expansion coefficient from the slope of the linear fitting of the linear relationship between (ΔL/L) and temperature. In this case, the linear thermal expansion coefficient was $\alpha = 5.5 \times 10^{-6}\ K^{-1}$.

Stability of $Rb_2Ti_{1.01}Er_{0.99}(PO_4)_3$ with the Temperature. Figure 5 shows the DTA thermogram of $Rb_2Ti_{1.01}Er_{0.99}(PO_4)_3$ in the 298−1473 K temperature range. There was a single peak at 1367 K. We did a more detailed study of this peak using X-ray powder diffraction, recording powder diffraction patterns at room temperature at the beginning and at the end of the experiment and at 50 K intervals between 1223 and 1473 K in heating and cooling cycles. Figure 6 shows the most interesting X-ray patterns obtained. At 1323 K a new phase begins to appear, identified as $ErPO_4$ (83-0662-JPDS database[16]). At 1373 K, there were new peaks corresponding to rutile (87-0920-JPDS database[16]), which may have appeared earlier because all of its peaks overlap with peaks of $Rb_2Ti_{1.01}Er_{0.99}(PO_4)_3$. In the last X-ray diffractogram at room temperature, the $Rb_2Ti_{1.01}Er_{0.99}(PO_4)_3$ phase did not appear. Instead, $ErPO_4$ and TiO_2 remained, which suggest that the decomposition of $Rb_2Ti_{1.01}Er_{0.99}(PO_4)_3$ is an irreversible process. From these data, we can propose a decomposition of $Rb_2Ti_{1.01}Er_{0.99}(PO_4)_3$ at a temperature of about 1323 K in accordance with this reaction:

$$Rb_2Ti_{1.01}Er_{0.99}(PO_4)_3 \rightarrow ErPO_4(s) + TiO_2(s) + Rb_2O(g) + P_2O_5(g)$$

SHG. The second-harmonic response of the $Rb_2Ti_{1.01}Er_{0.99}(PO_4)_3$ crystal was made using the powder method. We compared SHG efficiency (η), defined statistically as the power of the signal whose frequency is twice that of the initial radiation divided by the power of the initial beam, with the efficiency of other nonlinear optical crystals widely used in optical applications such as KTP and KDP. The results were $\eta/\eta_{KTP} = 0.21$ and $\eta/\eta_{KDP} = 1.28$. We can conclude that the second-harmonic generation is significantly less efficient than that of KTP, but

(15) Dowty, E. *Shape for Windows*, Version 5.0.1, Shape Software: Kingsport, USA. 1995.

(16) JCPDS-ICDD. Joint Committee of Powder Diffraction Standards-International Center for Diffraction Data, PA, 2000.

is of the order of KDP. As KDP is widely used in industrial applications, further studies of the growth conditions of larger single crystals for accurate optical measurements are justified.

Conclusions

We successfully grew langbeinite-type structures containing Ti^{4+} and Ln^{3+} ions as $M_2Ti_{2-x}Ln_x(PO_4)_3$ crystals ($M = K^+$ or Rb^+ and $Ln = Er^{3+}$ or Yb^{3+}) by high-temperature-solution methods. This creates possible new uses for these crystals, for example, as laser materials and self-doubling materials. The stability of this phase in the system $Rb_2O-P_2O_5-TiO_2$ is higher in relation to the higher the concentration of P_2O_5 in the solution and the lower the concentration of TiO_2 when only Ln_2O_3 is substituting TiO_2. When Nb_2O_5 is present, the langbeinite phase can be stabilized with a lower substitution of TiO_2 by Ln_2O_3. Also, as these compounds are not centrosymmetric, they can be used as nonlinear optical materials. This is shown by SHG studies in which the SHG efficiency is even higher than that of KDP. Our detailed structural study indicates that in langbeinite-type materials containing mixed-valence cations, which occupy two different positions in the framework, both cations are distributed in both positions. However, trivalent cations tended to occupy position 1. This structure expands as the temperature increases and has a linear thermal expansion coefficient of 5.5×10^{-6} K^{-1} in the 298−773 K range. This compound decomposes at 1323 K, to form $ErPO_4$ and TiO_2.

Acknowledgment. The authors acknowledge CIRIT for financial support of this work through the Project 2001SGR317 and CICyT through the Projects MAT99-1077-C02 and FIT-070000-2002-461. We also thank the Serveis Cientifico Tècnics of the Universitat de Barcelona for kindly supplying helpful measurements on EPMA. J. J.Carvajal would also like to acknowledge the grant he received from the Catalan Government (2000FI 00633 URV APTIND).

CM020806T